Symmetry effects on electron-transfer reactions: temperature dependence as a diagnostic tool

Y. Zeng, and M. B. Zimmt

More About This Article

The permalink http://dx.doi.org/10.1021/j100200a035 provides access to:

- Links to articles and content related to this article
- Copyright permission to reproduce figures and/or text from this article

Symmetry Effects on Electron-Transfer Reactions: Temperature Dependence as a Diagnostic Tool

Y. Zeng[†] and M. B. Zimmt*

Department of Chemistry, Brown University, Providence, Rhode Island 02916 (Received: April 2, 1992; In Final Form: June 11, 1992)

The temperature dependences of photoinduced intramolecular electron-transfer rate constants are used to determine the magnitude of the donor–acceptor electronic coupling matrix element, $|V|$, across seven σ bonds for three donor–spacer–acceptor molecules 1–3 in acetonitrile and tetrahydrofuran. The semiclassical formulation of electron-transfer rate constants and a linearized approximation are used to analyze the rate constants. Charge-transfer emission spectra from shorter analogs of 1 and 2 are analyzed to obtain estimates of the vibrational reorganization energy, the "average" vibration frequency, and S, the electron–phonon coupling constant, which are required in order to extract $|V|$ from the rate constant analyses. The results confirm predictions based on electronic symmetry arguments that electron transfer is symmetry forbidden in 1 and symmetry allowed in 2 and 3. In addition, the analyses suggest that through solvent coupling is more effective in acetonitrile than in tetrahydrofuran. Additional sources of the apparent solvent dependence of $|V|$ are discussed.

1. Introduction

The results from numerous investigations of electron-transfer (eT) reactions have demonstrated strong correlation between transfer rate constants and the free energy change of the reaction.[1,2] In line with Marcus' predictions,[3] electron-transfer rate constants increase sharply as the reaction driving force, $-\Delta G°$, increases from zero. A maximum in the transfer rate constant is achieved at a value of $-\Delta G°$ which depends on both the redox partners and the reaction environment.[1-4] In systems where diffusion is not rate limiting, transfer rate constants decrease as the reaction driving force is increased beyond this value.[1-4] Reactions whose thermodynamics and kinetics fall within this latter range are often said to be in the inverted region.

In principle, the "parabolic" dependence of transfer rate on reaction driving force provides a means for controlling electron-transfer dynamics and the yield of chemistry initiated by ion pairs.[1,2,5] Closs and Miller[4] have pointed out the advantage of effecting electron-transfer mediated, light to chemical energy storage in relatively nonpolar environments. High efficiency in such energy storage systems requires quantitative conversion of the excited state into the initial electron transfer product (ion pair) with minimal amounts of back transfer, reforming the neutral, ground state. Weakly exothermic, photoinduced charge separation reactions in nonpolar media can be very rapid and an efficient means for converting excited states into the ion pair state. By contrast, the reverse, charge recombination reactions may lie well into the inverted region and, as a consequence, proceed with diminished rate constants. Slow "back"-transfer increases the time for productive reactions of the ion pair state.

We have become interested in devising alternative means by which forward and reverse, non-adiabatic electron-transfer rate constants can be independently controlled.[6] Within golden rule formulations, the non-adiabatic electron-transfer rate constant is determined by the product of an electronic coupling matrix element squared, $|V|^2$, and a Franck–Condon weighted density of states (FCWDS).[7] The driving force dependence of electron-transfer rate constants is contained within the FCWDS. Electronic mixing of the initial and final diabatic states determines $|V|$. For *photoinduced* electron-transfer reactions, the magnitude of the electronic coupling between the excited (neutral) and charge-transfer (CT) states can be different from the magnitude of $|V|$ between the charge-transfer and ground (neutral) states. In a simple, one electron picture, $|V|$ for electron transfer from the photoexcited donor is determined by mixing of the donor's lowest unoccupied molecular orbital (LUMO) with the LUMO on the acceptor. In contrast, $|V|$ for the thermal, reverse transfer is determined by mixing of the acceptor LUMO with the donor's

highest occupied molecular orbital (HOMO).[8] Differences in the donor LUMO and HOMO wave functions can effect differential modulation of $|V|$ in the forward and reverse electron-transfer steps, respectively.[9] In a properly constructed system, a difference in the irreducible representation (electronic symmetry) with which the donor HOMO and LUMO wave functions transform may significantly reduce the coupling of one with the acceptor LUMO.

In a recent investigation, we examined the effect of electronic symmetry on the room temperature rate constants of photoinduced, intramolecular charge separation reactions.[6] The rigid, polycyclic donor–spacer–acceptor (DSA) molecules 1–3 (see Chart I) exhibit approximate C_s symmetry. The LUMO of the 1,1-dicyanoethylene acceptor in 2 and 3 is symmetric (a′), and the LUMO of the 1,2-dicarboethoxyethylene acceptor in 1 is antisymmetric (a″) with respect to the mirror plane symmetry element in these molecules. Electron transfer from the symmetric (a′) LUMO of the excited anthracene donor to the acceptor LUMO is formally symmetry allowed in 2 and 3 but formally symmetry forbidden in 1. In solvents more polar than diethyl ether, the electron-transfer rate constants in excited 2 and 3 were found to be 3-10 times faster than the transfer rate constants in 1, despite the greater exothermicity of transfer in the latter DSA. Values of $|V|$ in 1–3 were calculated from the rate constant data using a semiclassical formulation of eT rate constants, Marcus' equation[3] to estimate the solvent reorganization energy, λ_s, and literature estimates of both the vibrational reorganization energy, λ_v, and the vibrational spacing, $\hbar\omega$. In this manuscript, the temperature dependences of the eT rate constants in 1–3 and the charge-transfer emission spectra from analogs of these DSA's are analyzed to obtain *experimental* estimates of the reorganization parameters. Analyses of the eT rate data using the experimental values of the reorganization parameters allow more quantitative characterization of $|V|$. The results provide considerable evidence that electronic symmetry strongly modulates both $|V|$ and electron-transfer rate constants.

2. Experimental Section

Absorption spectra were recorded on either a Perkin Elmer 552A or Lamda 3B UV–vis spectrophotometer. Emission spectra were recorded using a SPEX F111XI fluorimeter system. Spectra were corrected for the response of the detection monochromator and phototube. Electrochemical measurements were performed in a 10-mL glass cell equipped with either a glassy carbon (1.5-mm radius) or Pt (100-μm radius) disk as the working electrode, a platinum wire as the counter electrode, and a Metrohm Ag/AgCl electrode filled with CH_2Cl_2/0.1 M tetrabutylammonium hexafluorophosphate ((TBA)PF_6) saturated with LiCl as the reference electrode. The reference electrode was separated from the test solution by a salt bridge containing the test solvent and 0.1 M (TBA)PF_6. The test solution contained the donor or acceptor

---

[†]Current address: Department of Chemistry, Brandeis University, Waltham, MA.

TABLE I: Temperature Dependent Decay Rate Constants of 4

ACN		THF	
T/K	$k°/(10^7 \text{ s}^{-1})$	T/K	$k°/(10^7 \text{ s}^{-1})$
296	2.29	295	3.53
273	2.32	271	3.56
256	2.28	238	3.52
238	2.28	216	3.53

models 5–7 (Chart I) and 0.1 M (TBA)PF$_6$ and was N$_2$ purged for 30 min prior to and during the measurement. Ferrocene was added as an internal reference following the collection of the electrochemical wave forms. Wave forms were recorded from at least three separate samples in each solvent.

The syntheses of the DSA molecules will be reported elsewhere. Prior to the fluorescence experiments, each compound was purified at least twice by chromatography on Analtech Silica Gel GF 1000-μm plates. Tetrahydrofuran was distilled from sodium-benzophenone ketyl through a 6-in. vigreux immediately prior to sample preparation. Acetonitrile was distilled from CaH$_2$ and used immediately. The concentrations of 1–4 were adjusted to provide an optical density of 0.05–0.10 at 317 nm in a 1-cm path length cell. Samples were degassed by four cycles of freeze-pump–thaw at 0.1 Torr and then transferred to a 3-mm path length quartz cell in a nitrogen flushed glovebag. The quartz cell was sealed and mounted onto an aluminum base which screwed into the cold stage of a High-Tran liquid-nitrogen-transfer system (R. G. Hansen Associates, Santa Barbara, CA). Thermal contact between the aluminum mount and the cold stage was facilitated with an indium gasket. A thin layer of Krytox fluorinated grease was placed between the base of the quartz cell and the aluminum mount to facilitate heat transfer. The radiation shield and vacuum shroud were attached, and the system was evacuated using a single stage rotary pump. The sample temperature was adjusted by controlling power to the tip heater using a feedback circuit driven by a thermocouple in contact with the cold stage. The temperature of the cell was monitored using a calibrated silicon diode temperature sensor which was placed in an indentation of the cell. The indentation was filled with Krytox grease to facilitate thermal contact. The sample temperature was allowed to equilibrate for 20 min prior to acquisition of the fluorescence decays. The temperature of the sample was maintained within ±1.0 °C during data acquisition.

The excitation source was the 317-nm doubled output of a home-built, electrooptically cavity dumped dye laser which was synchronously pumped by the doubled output of a mode-locked and Q-switched Nd:YAG (Antares 76S). The pulse width at 317 nm was less than 50 ps, and the pulse energy was 0.5–1.5 μJ in a spot size of 4 mm^2. The excitation pulse was vertically polarized. Sample fluorescence was collected in a backscattering geometry using a 25-mm-diameter, 50-mm-focal length suprasil lens, passed through a quartz polarizer set at 54.7° to the vertical, spectrally filtered using an ISA H-20 monochromator (5-nm band pass), and detected with a Hamamatsu R1645U-07 microchannel plate. The resulting wave form was recorded with a Tektronix 7912AD digitizer. A mechanical shutter blocked alternate laser shots to obtain a background wave form. This wave form was subtracted from the previous fluorescence wave form. Averages were obtained from 1000 to 2000 (fluorescence – background) wave forms. The system impulse response was recorded using a scattering sample. The laser repetition rate for all experiments was 3 Hz.

Decay rate constants were determined by nonlinear least squares fitting of the experimental wave form to the convolution of the
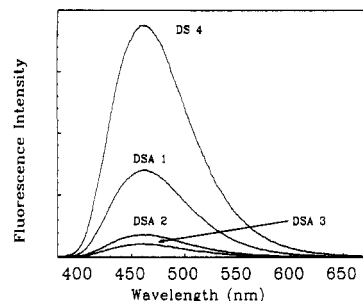

Figure 1. Emission spectra of 1–4 in THF excited at 350 nm. The optical density of all samples was 0.1 at the excitation wavelength.

system response with a single exponential decay. For each DSA and solvent, fluorescence decays were recorded as a function of temperature at two or more different wavelengths within the room temperature fluorescence band. At least two, independent determinations of the temperature dependence of the fluorescence decay rate constants were completed for each compound and solvent.

3. Results and Discussion

a. Donor Decay Rate Constants. In DSA's 1–3, electron transfer occurs from the excited, singlet state of the dimethoxyanthracene donor to the acceptor. In order to determine the electron-transfer rate constants, the excited-state decay rate constant of the donor in the absence of eT must be measured. The donor–spacer (DS) molecule 4 was used for this purpose. Two observations support the use of 4 as a relevant donor model. First, the fluorescence spectrum of 4 overlaps exactly with the normalized fluorescence spectra of 1–3 (Figure 1). This is not true for some of the shorter DS models we employed. Second, the decay rate constants of excited 4 and 2 are identical in alkane solvents. Electron transfer from the excited donor to the dicyanoethylene acceptor is endothermic in alkane solvents (vide infra) and does not occur within the excited-state lifetime. Thus, the temperature dependence of the donor excited-state lifetime in each solvent can be determined using DSA 4.

Table I lists the fluorescence decay rate constants of 4 in THF and acetonitrile (ACN) as a function of temperature. In ACN, the fluorescence lifetime increases by <1 ns between 296 and 238 K. The change is less than the statistical uncertainty of the individual measurements. In THF, the excited-state decay rate constant is essentially independent of temperature between 216 and 295 K. As previously noted, the dimethoxyanthracene excited-state lifetime is longer in ACN than in THF.[6] However, the decay processes are essentially unactivated in both solvents (<0.1 kcal/mol). Thus, for each solvent, the average of the values measured as a function of temperature will be used as the excited-state decay rate constant at all temperatures: 2.31 × 10^7 s^{-1} in ACN; 3.51 × 10^7 s^{-1} in THF.

b. Electron-Transfer Rate Constants. In contrast to 4, the excited-state decay rate constants of 1–3 exhibit measurable temperature dependences. The electron-transfer rate constants are determined according to eq 1, where $k_{T,X}$ is the decay rate

$$k_{eT} = k_{T,X} - k°_X \qquad (1)$$

constant of the excited donor in the DSA at temperature T in solvent X and $k°_X$ is the decay rate constant of the excited donor in DS 4 in solvent X. The eT rate constants for 1–3 are plotted as a function of temperature in Figure 2a–c. The eT rate constants at various temperatures in ACN and THF are listed in

TABLE II: Temperature Dependent Electron-Transfer Rate Constants[a] in 1–3

1-ACN		1-THF		2-ACN		2-THF		3-ACN		3-THF	
T/K	$k_{eT}/(10^7 \text{ s}^{-1})$	T/K	$k_{eT}/(10^7 \text{ s}^{-1})$	T/K	$k_{eT}/(10^7 \text{ s}^{-1})$	T/K	$k_{eT}/(10^7 \text{ s}^{-1})$	T/K	$k_{eT}/(10^7 \text{ s}^{-1})$	T/K	$k_{eT}/(10^7 \text{ s}^{-1})$
295	2.7	295	5.8	295	7.2	295	33	293	8.8	295	57
277	2.2	265	4.6	275	3.8	266	20	276	5.5	266	39
255	1.5	237	3.7	258	2.1	237	8.9	258	3.1	240	24
236	1.0	210	2.5	238	0.9	216	4.7	238	1.5	213	13

[a] The electron-transfer rate constant data at all temperatures investigated are available as supplementary material.

CHART I

1

2

3

4

5   **6**

7   **8**

9

10

Figure 2. Experimental and best fit calculated electron-transfer rate constants as a function of temperature. In each panel, the squares represent the electron transfer rate constants in THF; the crosses represent the electron transfer rate constants in ACN. See section 3f for a discussion of the calculated rate constants, Table V for the values of ΔG° and λ_s, and Table IV for the values of λ_v and $\hbar\omega$. (a, top) DSA 1 (S = 3.7); (b, middle) DSA 2 (S = 2.2); (c, bottom) DSA 3 (S = 2.2).
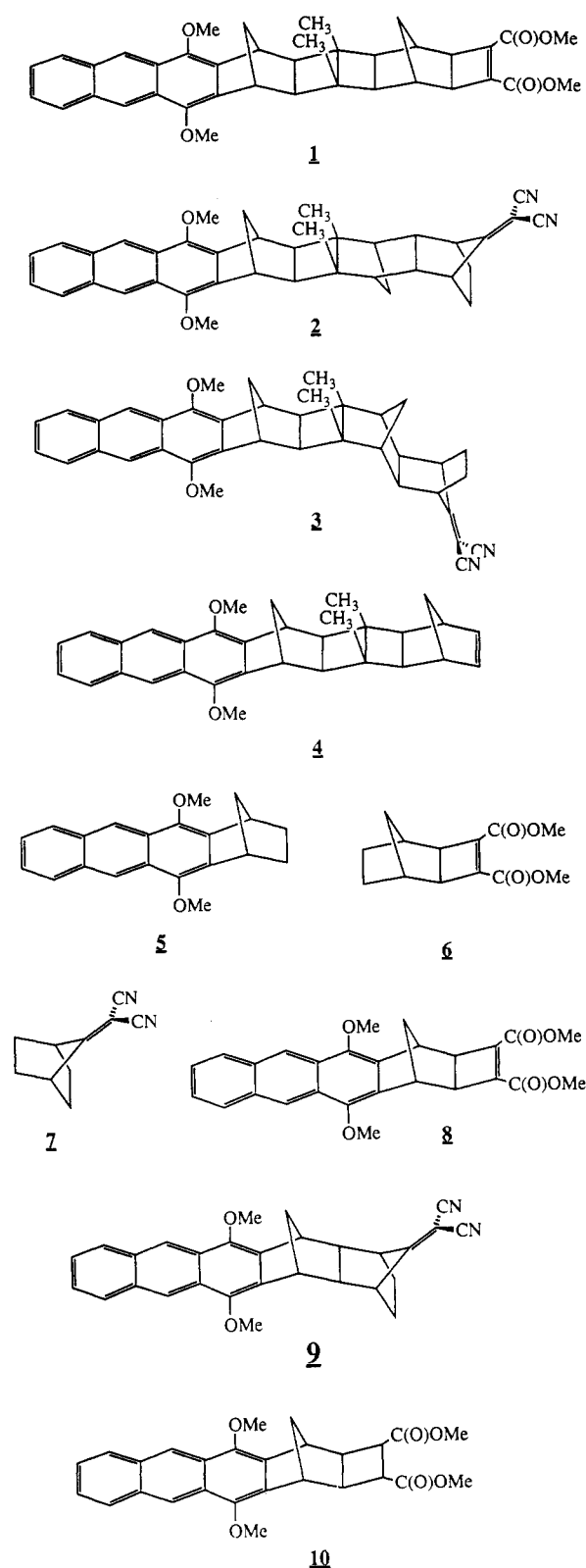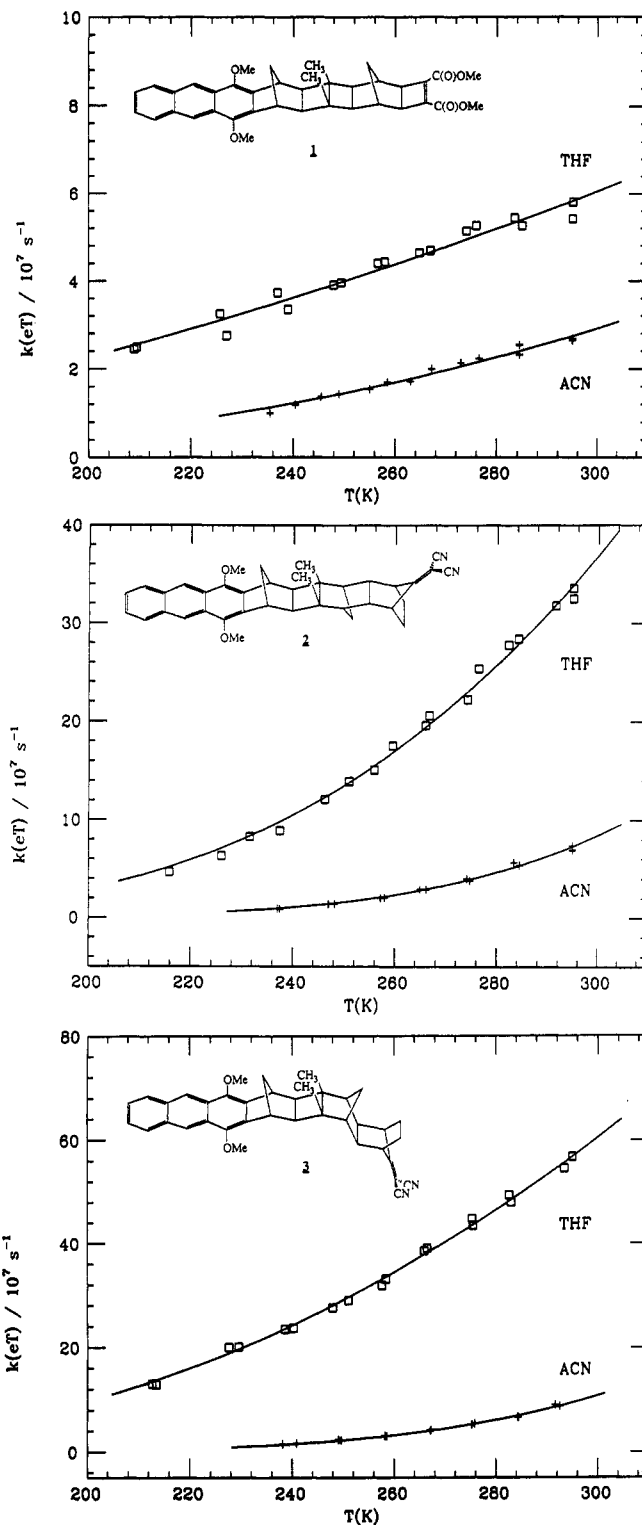
Table II. The ratio of the highest to the lowest temperature eT rate constants is smallest in **1** and largest in **2**. For each DSA, this rate constant ratio is larger in ACN than in THF, despite the larger temperature range used for the latter solvent. Near room temperature, electron transfer is faster in **2** and **3** than in **1**. The difference in rate constants decreases as the temperature is lowered. Clearly, the activation barrier for electron transfer is smallest in DSA **1**. In order to determine and compare the electronic coupling matrix elements in these DSA's, the FCWDS for each system must be evaluated.

c. Arrhenius Evaluation of the Temperature Dependence. Within the semiclassical formulation of electron-transfer rate constants, eq 2, it is the coupling matrix element $|V|$ which would be reduced in a symmetry forbidden DSA. Equation 2 is derived

$$k_{eT} = (\pi / \hbar^2 \lambda_s k_b T)^{1/2} |V|^2 \Sigma (e^{-S} S^j / j!) \exp(-[(\lambda_s + \Delta G^\circ + j\hbar\omega)^2 / 4\lambda_s k_b T]) \quad (2)$$

$$S = \lambda_v / \hbar\omega$$

TABLE III: Experimental and Calculated Electron-Transfer Parameters. Linear Analysis

DSA	$\Delta G°(S_1 \rightarrow CT)^a$/eV	E_a/eV	ln (intercept)	λ_s(expt)/eV	λ_s(calcd)^b/eV	S^c	$\lvert V\rvert^c$/cm^{-1}	S^d	$\lvert V\rvert^d$/cm^{-1}
in ACN									
1	−0.55	0.105	24.1	1.29	1.0	3.7	19	2.2	9.1
2	−0.27	0.233	30.1	1.41	1.1	2.2	180	2.9	250
3	−0.28	0.207	29.3	1.33	0.86	2.2	120	2.9	170
in THF									
1	−0.38	0.064	23.3	0.85	0.71	3.7	11	2.2	5.4
2	−0.08	0.149	28.4	0.74	0.78	2.2	66	2.9	92
3	−0.14	0.107	27.2	0.68	0.61	2.2	35	2.9	49

^{a}Calculated according to eq 4. E_{00}(THF) = 3.04 eV; E_{00}(ACN) = 3.00 eV. $R_{cc}(1)$ = 11.9 Å; $R_{cc}(2)$ = 12.1 Å; $R_{cc}(3)$ = 8.6 Å. r(donor) = 5.0 Å; r(acceptor in **2** and **3**) = 3.9 Å; r(acceptor in **1**) = 4.2 Å. ^{b}Calculated using Marcus' expression for λ_s and parameters as specified in a (see ref 3). ^{c}Assuming $\hbar\omega$ and λ_v from entries 3 and 5 in Table IV. ^{d}Assuming $\hbar\omega$ and λ_v from entries 1 and 4 in Table IV.

for the case of non-adiabatic electron transfer in which a single vibrational mode couples the reactant and product states. Furthermore, it is assumed that the harmonic force constant is the same in both states, that only the lowest vibrational level of the reactants is populated, and that the solvent modes can be treated classically. To first order, $\lvert V\rvert$ is independent of temperature. The majority of the temperature dependence in the eT rate constant derives from the Franck–Condon factors.[7a] Thus, analysis of the temperature dependent rate constants provides a means to separately determine $\lvert V\rvert$ and the FCWDS. For weakly exothermic electron-transfer reactions, a preliminary analysis[11] of the temperature dependence can be achieved by assuming that the CT state is formed only in its lowest vibrational state ($j = 0$ in eq 2). With this assumption, eq 2 reduces to an Arrhenius-like form, eq 3. The activation energy depends only on $\Delta G°$ and λ_s. The

$$k_{eT} = (\pi/\hbar^2\lambda_s k_b T)^{1/2}\lvert V\rvert^2 (e^{-S}) \exp(-[(\lambda_s + \Delta G°)^2/4\lambda_s k_b T]) \tag{3}$$

pre-exponential factor depends on temperature, $\lvert V\rvert$, λ_s, and the electron–phonon coupling, S ($\lambda_v/\hbar\omega$). Provided λ_s and S are not vastly different for two DSA's, the ratio of their pre-exponential factors provides an estimate of the relative magnitudes of $\lvert V\rvert^2$.

Plots of $(T^{1/2} \ln k_{eT})$ vs $1/T$ for **1–3** in THF and ACN are presented in Figure 3a–c. With the exception of DSA **2** in THF, the plots show little systematic deviation from the best fit straight line. For each DSA, the activation energy is larger in ACN (Table III). In both solvents, the activation energies increase in the order **1 < 3 < 2**. Most significantly, in THF and ACN, respectively, the pre-exponential factor (intercept) is 180 and 400 times larger for **2** than for **1** and 3 and 2 times larger, respectively, for **2** than for **3** (Table III).

According to eq 3, λ_s can be obtained from the slopes provided $\Delta G°$ is known. Such analyses must be undertaken with considerable skepticism, for, as pointed out by Michel-Beyerle, both λ_s and $\Delta G°$ vary with temperature.[11] Liang et al. reported that λ_s for transfer across a steroid in methyltetrahydrofuran increased by 23% for a drop of 190 K.[12] In charge separation reactions, $\Delta G°$ decreases as the temperature is lowered (vide infra). If we assume the temperature dependence of λ_s is the same for charge shift[12] and charge separation reactions, then λ_s and $\Delta G°$ change in opposite directions as the temperature is varied. Our efforts to effect an analysis in which λ_s and $\Delta G°$ varied with temperature were unsuccessful. Thus, we proceed with the analysis in which λ_s and $\Delta G°$ are assumed to be temperature independent, having stated the caveat.

$\Delta G°$ for the photoinduced transfers is calculated using eq 4. The redox potentials were measured in ACN.[13] $E_{ox} - E_{red}$ in THF is calculated using the redox potentials from ACN and the Born equation.[14] The excited-state energies, E_{00}, in THF and ACN were previously estimated.[6] The point charge coulomb model is used to evaluate electrostatic interactions in the CT state. The estimates of $\Delta G°$ from eq 4 are listed in Table III.

$$\Delta G° = -E_{00} + (E_{ox} - E_{red}) - e^2/\epsilon_s R_{cc} \tag{4}$$

The values of λ_s derived from the experimental activation energies and $\Delta G°$ are listed in Table III along with values calculated with Marcus' continuum model[3a] (see footnote a in Table III for
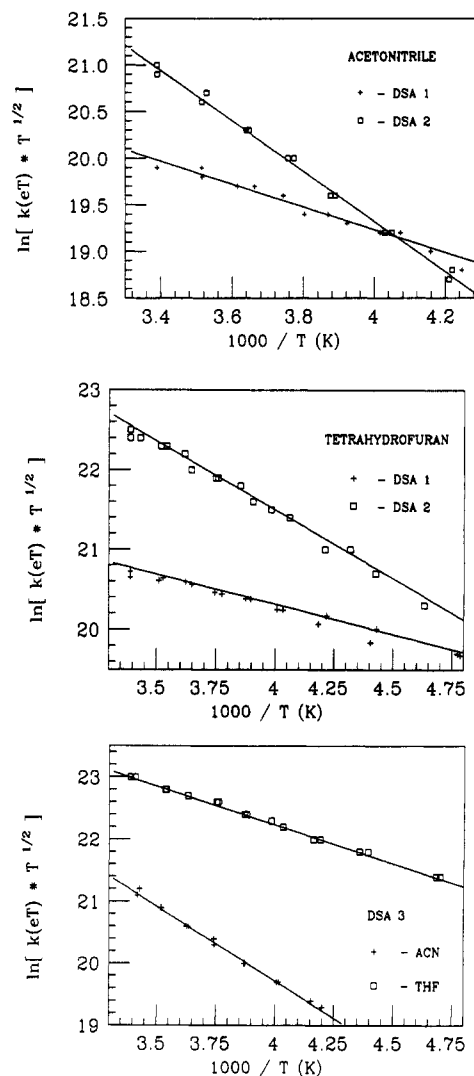

Figure 3. Arrhenius analyses of the temperature dependent electron-transfer rate constants. The determination of the best linear fit is discussed in section 3c. (a, top) DSA **1** (+) and DSA **2** (□) in ACN; (b, middle) DSA **1** (+) and DSA **2** (□) in THF; (c, bottom) ACN (+), THF (□) in DSA **3**.

the parameters). The experimental λ_s in ACN are 25–85% larger than the calculated values. By contrast, the experimental values of λ_s in THF are in reasonable agreement with the predictions of the dielectric continuum model, ranging from 6% smaller to 16% larger. Given the uncertainties in the slopes and $\Delta G°$, particularly in THF, the values of λ_s for **1** and **2** in each solvent should be considered indistinguishable. Surprisingly, λ_s for **2** and **3** are also nearly equal. The continuum model predicts a 25% decrease from **2** to **3**. However, use of the continuum model to calculate λ_s is least appropriate in **3** as the donor and acceptor are proximate, separated by one or two solvent molecules at most. Furthermore, accurate estimation of $\Delta G°$ (and thus λ_s) is particularly difficult for **3** for similar reasons. Despite these diffi-

TABLE IV: Electron-Transfer Parameters from Analyses of the Charge-Transfer Emission Spectra

entry	λ_v/eV	$\hbar\omega$/cm^{-1}	S	$\Delta G°$(MCH)/eV	λ_s(MCH)/eV	SSE(MCH)[a]	$\Delta G°$(Et$_2$O)/eV	λ_s(Et$_2$O)/eV	SSE(Et$_2$O)[a]
in DSA 8									
1	0.39	1410	2.2	−2.8	0.32	0.008	−2.7	0.45	0.028
2	0.43	1350	2.6	−2.8	0.25	0.010	−2.6	0.38	0.028
3 (AM1)	0.53	1150	3.7	−2.8	0.13	0.012	−2.6	0.25	0.027
in DSA 9									
4	0.50	1400	2.9				−3.0	0.64	0.011
5	0.42	1530	2.2				−3.1	0.79	0.011
6 (AM1)	0.31	1780	1.4				−3.2	1.04	0.013

[a] SSE is the sum of the squared residuals obtained from the fit of the calculated to the experimental CT emission spectrum. The experimental spectra were scaled to 1.0.

culties, we will use the experimentally derived values of λ_s in the remainder of this analysis.

It is interesting to note that λ_s for 1–3 in ACN lie inbetween λ_s reported for contact ion pairs (CIP) and solvent separated ion pairs (SSIP) in ACN.[15] In the CIP, solvent is excluded from the space between the ions. In addition, the proximity of the oppositely charged ions leads to a reduction in their interactions with the solvent (λ_s = 0.55 eV). In the SSIP, solvent surrounds each ion leading to significantly larger interactions (λ_s = 1.72 eV). In DSA's 1 and 2, the spacer excludes solvent from the volume directly between the donor and acceptor. However, the ion fields interact strongly with the large volume of solvent at the periphery of the spacer. More accurate calculations of λ_s and $\Delta G°$ for these DSA's could be obtained through use of ellipsoidal cavity models,[16] but we have not investigated these approaches at this time.

As mentioned previously, the intercepts of the plots in Figure 3 are 2 orders of magnitude larger for 2 than for 1. The intercepts may be equated to $|V|^2 e^{-S}(\pi/\hbar^2\lambda_s k_b)^{1/2}$, where k_b is Boltzmann's constant. $|V|$, λ_s, and e^{-S} vary as a function of DSA structure. The experimental values of λ_s in 2 and 3 demonstrate that solvent reorganization is not responsible for the large difference in the intercepts. Since S, which equals $\lambda_v/\hbar\omega$, appears as an exponent, it can exert a large influence on the magnitude of the intercept. If S in 1 is 5 larger than S in 2, vibrational reorganization, not electronic symmetry, could be responsible for the 100-fold difference in the intercepts. However, most literature estimates of S in organic systems are less than 4. Thus, the large difference in the intercepts for DSA's 2 and 3 provides qualitative support for symmetry effects on electron-transfer reactions. A more quantitative analysis requires determination of S.

d. Analysis of Charge-Transfer Emission Spectra. Recently, Marcus reformulated models for charge-transfer absorption and emission spectra to incorporate classical solvent and quantized vibrational modes.[17] Simultaneous analysis of *both* charge-transfer spectra allows evaluation of the four parameters entering into the semiclassical FCWDS; λ_s, λ_v, $\hbar\omega$, and $\Delta G°$. With only one of the two spectra, it is possible to obtain estimates of these parameters.[15b]

The emission spectra of DSA's 1–3 (Figure 1) consist of a single band which originates from the excited donor. Charge-transfer emission bands were not observed from these DSA's in any solvent. The emission spectra from the related DSA's 8 and 9 contain a second, longer wavelength, short lived, broad emission band. On the basis of the large Stokes shifts observed with increasing solvent polarity, these bands are assigned as emissions from the charge-transfer state. The CT spectra (Figure 4) from DSA 8 in methycyclohexane (MCH) and ether and from DSA 9 in ether have been isolated by subtracting the appropriately scaled emission spectrum of DS 10 from that of the DSA. DSA 9 exhibits no CT emission in alkane solvents. In THF, the charge-transfer emission bands from 8 and 9 are very weak and extend too far into the red for accurate determination with our fluorimeter.

The CT spectra from 8 and 9 have been fit using Marcus' model[17] in an attempt to determine λ_v and $\hbar\omega$ (S) for use in analyzing the electron-transfer kinetics from 1 and 2, respectively. Since the width of the calculated spectrum responds strongly to $\hbar\omega$, numerous initial values were employed in the fitting (1350–1600 cm^{-1}). Unfortunately, numerous (λ_v, $\hbar\omega$) pairs produce excellent fits to the CT emission spectra from 8 in both
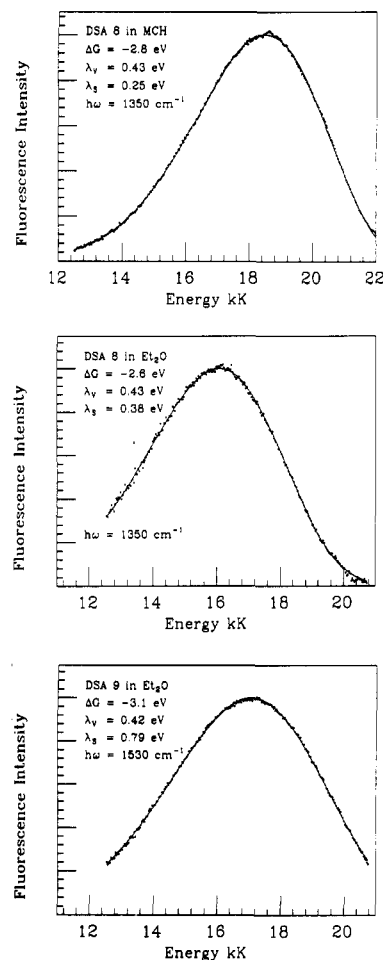

Figure 4. Experimental and best fit calculated charge-transfer emission spectra. The contribution of emission from the S$_1$ state has been subtracted. See section 3d for the discussion of the calculated spectra. (a, top) DSA 8 in MCH; (b, middle) DSA 8 in Et$_2$O; (c, bottom) DSA 9 in Et$_2$O.

MCH and ether. The values of $\Delta G°$, λ_s, λ_v, and $\hbar\omega$ for the two best fits to both CT emission spectra from 8 are listed as entries 1 and 2 in Table IV. Entry 3 in Table IV lists $\Delta G°$, λ_s, and $\hbar\omega$ obtained from fits of the CT emission spectra from 8 using a value of λ_v determined in AM1 calculations (vide infra).

The $\Delta G°$'s extracted from the above three fits are in reasonable agreement with estimates obtained from the redox potentials, Coulomb stabilization, and Born corrections; DSA 8, −2.9 ± 0.1 eV in MCH and −2.6 ± 0.1 eV in ether. The corresponding estimates of λ_s are larger than would be expected from Marcus' continuum expression.[3a] For example, the continuum expression predicts λ_s = 0 in MCH. However, using this value, the calculated CT emission spectrum is highly structured. At least two factors contribute to the absence of structure in the observed CT emission spectrum and to the nonzero values of λ_s from the fitting. (1) Displacements and reorganization occur in low frequency modes of the solvent and spacer not included in the continuum models. Nonpolar solvents respond to strong fields, present in the CT state,

TABLE V: Experimental and Calculated Electron-Transfer Parameters. Nonlinear Analysis

DSA	$\Delta G°(S_1 \rightarrow CT)^a$/eV	S^b	λ_v(expt)^b/eV	$|V|^b$/cm^{-1}	S^c	λ_v(expt)^c/eV	$|V|^c$/cm^{-1}
in ACN							
1	−0.55	3.7	1.15	7.3	2.2	1.22	5.6
2	−0.27	2.2	1.36	125	2.9	1.38	160
3	−0.28	2.2	1.33	110	2.9	1.32	140
in THF							
1	−0.38	3.7	0.74	4.8	2.2	0.79	3.5
2	−0.08	2.2	0.70	47	2.9	0.70	62
3	−0.14	2.2	0.66	29	2.9	0.65	38

^{a}Calculated according to eq 4. E_{00}(THF) = 3.04 eV; E_{00}(ACN) = 3.00 eV. R_{cc}(1) = 11.9 Å; R_{cc}(2) = 12.1 Å; R_{cc}(3) = 8.6 Å, r(donor) = 5.0 Å; r(acceptor in 2 and 3) = 3.9 Å; r(acceptor in 1) = 4.2 Å. ^{b}Assuming $\hbar\omega$ and λ_v from entries 3 and 5 in Table IV. ^{c}Assuming $\hbar\omega$ and λ_v from entries 1 and 4 in Table IV.

by aligning the maximum component of the molecular polarizability tensor along the dipole field lines. In addition, the density of solvent in the vicinity of the CT state will be different than for the neutral state (electrostriction).[18] These motions contribute to the solvent reorganization energy as they alter the energy and occur with finite time constants. (2) The vibrational spectrum contains modes of many different frequencies which are coupled to the CT emission. The real density of vibrational states is much higher than that contained in the single high frequency mode, semiclassical model.[7,17] CT spectra calculated using this model cannot be made featureless by virtue of a high density of vibrational states. Instead, structureless spectra may be simulated by using large values of the solvent reorganization energy. As a consequence, when real CT spectra are simulated using this model, the estimated values of the solvent reorganization energy are too large. On the basis of fits of alkyl substituted naphthalene and anthracene fluorescence spectra, unresolved vibrational structure may contribute as much as 0.1 eV to λ_s in the CT spectra.[19]

The CT spectrum of DSA 9 in ether is also satisfactorily reproduced by numerous (λ_v, $\hbar\omega$) pairs (entries 4 and 5 in Table IV). Entry 6 in Table IV lists $\Delta G°$, λ_s, and $\hbar\omega$ obtained from a fit of the CT emission spectrum from 9 using a value of λ_v determined in AM1 calculations (vide infra). For some of these pairs, the accompanying best fit values place the CT-state energy above the local excited state ($\Delta G° < -3.1$ eV[6]) or require values of λ_s that are much larger than estimates based on Marcus' expression, as well as being larger than the experimental values of λ_s for the longer DSA's 1–2 in THF, a more polar solvent. Thus, we reject (λ_v, $\hbar\omega$) pairs which require $\Delta G°$ more negative than −3.1 eV or λ_s greater than 0.8 eV to reproduce the CT emission spectrum of 9 in ether. For the remaining (λ_v, $\hbar\omega$) pairs, the difference in $\Delta G°$ for 8 and 9 in ether is consistent with the ~0.3 eV more negative reduction potential of the dicyanoethylene acceptor.[20]

On the basis of these analyses of the CT emission spectra, λ_v for DSA 1 is between 0.39 and 0.53 eV and S lies within the range 2.2–3.7. For DSA's 2 and 3, λ_v is between 0.42 and 0.50 eV and S lies within the range 2.2–2.9. In the nonlinear analyses of the temperature dependent electron-transfer rate constants, we will use $S = 3.7$ (entry 3, Table IV) for DSA 1 and $S = 2.2$ for DSA's 2 and 3 (entry 5, Table IV). This choice, of the largest value of S for DSA 1 and the smallest acceptable value of S for DSA 2, generates the smallest $|V|(2)/|V|(1)$ ratio from the analysis of the rate constants, and, thus, establishes a lower limit on the magnitude of the symmetry effect in these DSA's.

Using λ_s obtained from the activation energies and λ_v and $\hbar\omega$ from the CT emission analyses, $|V|$ may be determined from the temperature dependence intercepts in Figure 3. As shown in column 8 of Table III, when the above estimates of S for 1–3 are used, $|V|(2)$ is 6–9 times larger than $|V|(1)$. $|V|(3)$ is 1.5–1.9 times smaller than $|V|(2)$. Further discussion of the $|V|$'s will be presented following the analyses employing the full semiclassical equation.

e. AM1 Calculation of Vibrational Reorganization Energies. In an attempt to provide independent estimates of λ_v for the photoinduced and electron-transfer back-reactions, AM1 semiempirical calculations[21] have been performed on the donor and acceptor portions of the DSA's.[22] The calculated difference in

the enthalpy of formation of neutral dicyanoethylene in the lowest energy anionic and neutral geometries, λ_v, is 0.13 eV. The calculated difference in the enthalpy of formation of the dicyanoethylene radical anion in the lowest energy neutral and anionic geometries, λ'_v, is very similar, 0.12 eV. The corresponding values, λ_v and λ'_v, for the anthracene donor are 0.19 and 0.18 eV. The largest geometric distortions accompanying the formation of the cation include shortening of the aryl–oxygen bond lengths, a 20° rotation of one of the methyl groups about the aryl–oxygen bond, and alternating compressions and extensions of the C–C bonds composing the substituted anthracene ring. The calculated value of λ_v for the dicarbomethoxyethylene acceptor is 0.25 eV. The dihedral angles between the carbonyl and alkene groups decrease from 23° and 48° in the neutral to 8° and 2° in the anion. In contrast to the donor and dicyanoethylene acceptor, λ'_v for the ester anion is distinctly different (0.44 eV) than for the neutral. The torsion potential in the dihedral angle composed of the C=C and C=O units is stiffer in the anion than in the neutral. The anion resists loss of conjugation more strenuously than the neutral resists planarization. In the absence of more detailed information, the average of λ'_v and λ_v will be used for all three groups. With this approximation, the total calculated λ_v for DSA 1 is ~0.53 eV and for DSA 2 or 3 is ~0.31 eV.

Using $\lambda_v = 0.53$ eV, the best fits to the CT spectrum from DSA 8 in MCH and ether require $\hbar\omega = 1150$ cm^{-1}. Typically, values between 1400 and 1500 cm^{-1} are employed for organic systems.[1,2] The corresponding values of λ_s and $\Delta G°$ are reasonable (Table IV, entry 3). The agreement between the experimental and calculated CT emission spectra using the AM1 based parameters is, however, not as good as with the prior entries in Table IV. Using $\lambda_v = 0.31$ eV to fit the CT spectrum from DSA 9 in ether requires $\hbar\omega = 1775$ cm^{-1}, $\lambda_s > 1.0$ eV, and $\Delta G° = -3.2$ eV. The latter two values are unreasonable for this DSA (vide supra). Furthermore, the other parameter sets listed in Table IV provide more accurate simulations of the observed CT spectrum. Thus, we have not used the AM1 based analysis for DSA's 2, 3, and 9.

f. Nonlinear Fitting of k_{eT} versus Temperature. Despite the relatively small exothermicities for photoinduced electron-transfer reactions in 1–3, vibrationally excited levels of the charge-transfer state can be populated. Ignoring electron transfers which populate vibrationally excited CT levels underestimates the Franck–Condon factors and produces an estimate of $|V|$ that is too large. Thus, the temperature dependences of the electron-transfer rate constants have been fit to eq 2 using a nonlinear least squares algorithm. Only λ_s and $|V|$ are determined by the program; the values of λ_v, $\hbar\omega$, and $\Delta G°$ are held constant. For each DSA and solvent, values of λ_s and $|V|$ have been determined using $\Delta G°$ within ±0.15 eV of the value in Table III.[23] Columns 4 and 5 in Table V list the values of λ_s and $|V|$ obtained using S listed in column 3. The solid lines in Figure 2 are the best fit calculated electron-transfer rate constants for each DSA and solvent as a function of temperature. The estimates of λ_s from the linear and nonlinear analyses are nearly identical. By contrast, the estimates of $|V|$ from the analyses using the full semiclassical equation are smaller than $|V|$ determined using the approximations in eq 3. This is consistent with an increase in the magnitude of the FCWDS.

g. Discussion. **(i) Symmetry Effects.** The results of the analyses

using eq 2 indicate that electronic coupling between the donor and acceptor in DSA **2** is significantly larger than in DSA **1**. $|V|(2)$ is 10 times larger than $|V|(1)$ in THF and 17 times larger than $|V|(1)$ in ACN (column 5, Table V). There are two possible origins of the larger $|V|$ in **2**. First, the edge fused 6:4:4:6:4 ring system within the spacer of **1** may be intrinsically less effective than the edge fused 6:4:6:5 ring system in **2**. Second, the reduction in $|V|$ may be a consequence of electronic symmetry. We are not aware of data in the literature that support the former explanation. Thus, the >10-fold reduction of $|V|$ from **2** to **1** is evidence for electronic symmetry effects in photoinduced electron-transfer reactions. This ratio of $|V|$'s translates into a 100–290-fold faster, optimal[24] electron-transfer rate constant in a symmetry allowed DSA relative to a symmetry forbidden DSA with the same donor and acceptor.

The principal challenge to the conclusions regarding symmetry effects in these DSA's is the inability to obtain a unique value of S. However, even if one uses λ_v's from the AM1 calculations and the corresponding $\hbar\omega$'s from the CT emission analyses to determine S for both DSA's (entries 3 and 6 in Table IV), the ratio $|V|(2)/|V|(1)$ obtained upon analysis of the temperature dependent rate data (using eq 2) is 7 in THF and 12 in ACN. This still represents a significant effect of symmetry on electron-transfer rate constants. If the temperature dependent electron-transfer rate constants are analyzed using the values of λ_v and $\hbar\omega$ that give the best fits of the charge-transfer emission spectra (entries 1 and 4 in Table IV), the ratio $|V|(2)/|V|(1)$ is 17 in THF and 27 in ACN (columns 6–8, Table V). This ratio of $|V|$'s translates into a 290–800-fold faster optimal[24] electron-transfer rate constant in the symmetry allowed DSA. These analyses demonstrate that electronic symmetry can alter electron-transfer rate constants by 2–3 orders of magnitude.

In studies of charge shift reactions, Closs and Miller found that the electronic coupling matrix elements across seven bonds in 2,6-disubstituted decalins vary from 13 to 30 cm^{-1}, depending on the stereochemistry of the donor and acceptor connections to the spacer.[4b] These numbers lie between our estimates of $|V|$ in the symmetry allowed and forbidden DSA's. Of course, the absolute magnitude of $|V|$ depends upon the orbital coefficients of the donor and the acceptor at the point of attachment. Nonetheless, the large range of $|V|$ spanned by DSA's **1** and **2** demonstrates the significance of the symmetry effect.

In essence, symmetry effects are a special case of the orientation dependence of $|V|$.[26] The introduction and use of electronic symmetry simplifies the task of identifying structures for which $|V|$ should be small. The rigidity of the spacers in DSA's **1–3**, and their connections to the donor and acceptor reduce the set of relative orientations that can be accessed by the neutral redox partners. In a related study, Helms et al. determined electron-transfer rate constants between two porphyrins as a function of the dihedral angle between the rings.[26d] The porphyrins were attached to the spacer by single bonds, and their relative orientations were fixed by nonbonded contacts between the spacer and the porphyrins. From their analysis, it appears that $|V|$ decreases by a factor of 4 between the allowed (0 and 90°) and forbidden (45°) geometries. This ratio of $|V|$'s is smaller than that observed between DSA's **2** and **1**. As the same donor and acceptor porphyrins were used at each dihedral angle, the interpretation of their kinetics is not complicated by different values of S. However, their spacers may not restrict the donor and acceptor porphyrin motions to as great an extent as those in DSA's **1** and **2**. Although steric effects constrain the dihedral angle between the porphyrin rings, fluctuations on the order of 5° may significantly reduce the apparent size of the orientation effect.

(ii) Solvent Dependence of $|V|$. The large solvent dependence of $|V|$ in DSA's **1–3** is quite unexpected. To the extent that donor–acceptor electronic interactions in the all trans DSA's are mediated primarily through the spacer σ bonds,[4b,25] $|V|$ should be solvent independent. Even in the bent DSA, **3**, the increase in $|V|$ of ~80 cm^{-1} from THF to ACN is larger than would have been expected (vide infra). In fact, Oliver et al.[25f] concluded that through solvent interactions are *smaller* in ACN than in THF,

based on a study of solvent effects on photoinduced electron-transfer rate constants in DSA's similar to **1–3**. We reached a similar conclusion in our initial solvent dependence studies of DSA's **1–3**.[6] However, as rate constants were measured only at room temperature, the conclusions were based on estimated Franck–Condon factors which, in our case, significantly underestimated the activation barrier to transfer in ACN. We propose two explanations for the apparent solvent dependence of $|V|$. The first is more interesting but, unfortunately, applies only to transfer in the symmetry forbidden DSA.

(i) In the symmetry forbidden DSA, $|V|$ increases with increasing reaction exothermicity. This can be understood by reference to the semiclassical model in eq 2. In the symmetry forbidden DSA, the purely electronic $|V|$ is exactly zero since the locally excited and CT states have opposite electronic symmetries, A″ and A′, respectively. The symmetry of the lowest vibronic level of the locally excited state is also A″. However, vibronic levels of the CT state in which an antisymmetric vibration is populated by an odd number of quanta have A″ symmetry.[27] Symmetry considerations no longer restrict $|V|$ to zero for the interaction of these levels with the lowest vibronic level of the excited state.[28]

Using a harmonic oscillator to simulate an antisymmetric vibration of the spacer and parallel ethylene π and π^* orbitals to represent the donor and acceptor LUMO's, respectively, one can readily demonstrate that $|V|$ is small, but nonzero, for transfer accompanied by a change of $2n + 1$ quanta ($n = 0, 1, 2, ...$) in the antisymmetric vibration. Furthermore, the vibronic $|V|$ increases with n. Thus, for the symmetry forbidden DSA, $|V|$ is dependent on j, the number of quanta in the accepting mode in eq 2. If the model employed assumes that $|V|$ is independent of j (as in eq 2), then the apparent magnitude of $|V|$ will increase as the higher vibronic levels of the CT state are more extensively populated, i.e., as the electron-transfer reaction becomes more exothermic. This argument can be extended to incorporate population in excited vibronic levels of S_1 or formation of the CT state with numerous quanta in symmetric and antisymmetric vibrations. The preceding explanation can be used to rationalize the increase of $|V|$ in **1** from 4.8 cm^{-1} in THF to 7.3 cm^{-1} in ACN. Unfortunately, $|V|$ in **2** and **3** exhibit even larger solvent dependences. These cannot be explained on the basis of symmetry considerations.

(ii) The temperature dependences of λ_s and $\Delta G°$, which appear in the sum of exponentials in eq 2, may not cancel. Furthermore, the mismatch in temperature dependences may be different in ACN and THF. Both the linear and nonlinear analyses presented here generate incorrect values of $|V|$ when the temperature dependences of λ_s and $\Delta G°$ are ignored. In a recent pulse radiolysis study of charge shift reactions, Liang et al.[12] presented two calculated curves of ln $(k_{eT}T^{1/2})$ versus $1/T$. In one calculation, the temperature dependences of λ_s and $\Delta G°$ were taken into account. In the other, λ_s was fixed at the room temperature value. The intercepts of the two curves differed by ~0.8 log units. The $|V|$'s extracted from these intercepts would vary by a factor of ~2.5. In the pulse radiolysis studies, $\Delta G°$ was only weakly dependent on temperature. The reactions of DSA's **1–3** should exhibit significantly larger temperature dependences in $\Delta G°$ as a pair of neutral species is converted into an ion pair ($\Delta S°$ is more negative). $\Delta S°$ for intermolecular electron transfer from a neutral donor to a neutral acceptor in ACN is ~–17 eu.[29] If the same entropy change is assumed for DSA's **1–3**, $\Delta G°$ in ACN becomes more exergic by 0.044 eV for a drop in temperature of 60 K. We do not have the data necessary to estimate the change of λ_s or the real change of $\Delta G°$ with temperature in these solvents. We are currently investigating the temperature dependence of charge-transfer emission spectra in analogous DSA molecules with the goal of determining the variation of λ_s and $\Delta G°$. At this point, we can only surmise that the <2.7-fold decrease in $|V|(1)$ and $|V|(2)$ from ACN to THF derives from improper treatment of λ_s and $\Delta G°$ as a function of temperature.

Having stated this conclusion regarding **1** and **2**, the nearly 4-fold reduction in $|V|(3)$ from ACN to THF is of interest (Table

V). In contrast to **1** and **2**, through solvent electronic coupling could constitute the largest contribution to $|V|$ in DSA **3**. Studies by Miller and others have established considerable precedent for through solvent coupling.[30] Only in DSA **3** is there a short and direct path from the donor to the acceptor that passes through the solvent. Furthermore, Verhoeven and collaborators have demonstrated that the presence of a gauche link (a bend) in a spacer reduces through bond contributions to electron-transfer rate constants by as much as an order of magnitude.[25f] These authors also concluded that through solvent electronic coupling can be comparable to through bond coupling in DSA's with bent spacers.[25f]

On the basis of Verhoeven's results,[25f] one gauche link in a spacer reduces through bond coupling by a factor of ~ 3 relative to an all trans spacer. The ratio $|V|(2)/|V|(3)$ is 1.6 in THF and 1.1 in ACN, both significantly less than 3. This is readily explained if through solvent contributions to $|V|$ in **3** are comparable to through bond contributions in **2** and much larger than through solvent contributions in **2**. If this interpretation is correct, the results from DSA's **2** and **3** demonstrate that through solvent coupling is *larger* in ACN than in THF. This proposal is consistent with superexchange models[9a,b] for $|V|$, in which lower lying antibonding orbitals are more effective at promoting electronic coupling. The π^* orbital of the nitrile is at a lower vertical energy than are the σ^* orbitals of THF. The other factors which determine $|V|$ in the superexchange model are the site-to-site coupling matrix elements. Through space "jumps" yield smaller site coupling matrix elements relative to through bond steps.[31] The short distance from the donor to the acceptor in DSA **3** does not require many through space jumps between solvent molecules. Thus, through solvent coupling could be more efficient in ACN than in THF for this DSA. From studies of related DSA's, Verhoeven[25] concluded that through solvent coupling is particularly effective in benzene. Similarly, in a recent investigation of ion pair formation dynamics, Gould and Farid[32] concluded that through solvent coupling is more effective in *o*-dichlorobenzene than in methylene chloride. If these effects can be attributed to low lying π^* orbitals in the solvent, similar arguments in ACN are not unreasonable. It would be particularly interesting to compare electron-transfer rate constants and $|V|$'s for **3** in ACN, toluene, and toluonitrile.

4. Conclusion

Accurate determination of intramolecular electronic coupling matrix elements from the temperature dependences of photoinduced electron-transfer rate constants requires considerable information in addition to the kinetics measurements: (1) the temperature dependences of the reaction driving force and the solvent reorganization energy must be known; (2) reliable estimates of the vibrational reorganization energy and the frequency of the vibration which is most affected by transfer must be determined. The analyses in this paper are based on the semiclassical model of electron-transfer rate constants in conjunction with the following approximations: (1) the reaction driving force and the solvent reorganization energy are independent of temperature; (2) vibrational reorganization energy and the corresponding vibration frequency appropriate to the photoinduced charge-transfer reaction can be determined from an analysis of the charge-transfer emission spectrum. Within this framework, these results demonstrate that electronic symmetry can significantly modulate photoinduced electron-transfer rate constants. Rate constant restrictions of at least 2 orders of magnitude are possible in appropriately constructed supramolecular structures. The symmetry effects observed in the photoinduced charge-transfer reactions are consistent with other investigations of orientation effects on electron-transfer reactions. DSA molecules **1–3** generated no detectable charge-transfer emission, thus precluding our investigation of symmetry effects on the charge recombination kinetics. Currently, we are attempting to determine, spectroscopically, the temperature dependence of the reaction driving force and solvent reorganization energies in related DSA's. We are also constructing a second generation of allowed and forbidden DSA molecules with identical or nearly identical donors and acceptors.

Evidence of both through bond and through solvent electronic coupling in intramolecular electron-transfer reactions has been presented. The through solvent contribution is particularly important for DSA **3**, which contains a short, direct through solvent path from the donor to the acceptor. Furthermore, the results suggest that through solvent coupling may be more efficient in acetonitrile than in tetrahydrofuran. In related DSA structures, other investigators have arrived at the opposite conclusion.[25f] If suffices to say that the quantitative relationships between structure, solvent, and the magnitude of through solvent electronic coupling have yet to be unambiguously determined.

Supplementary Material Available: Table of electron-transfer rate constants for DSA's **1–3** (2 pages). Ordering information is given on any current masthead page.

References and Notes

(1) (a) Rehm, D.; Weller, A. *Isr. J. Chem.* **1970**, *8*, 259. (b) Miller, J. R.; Beitz, J. V.; Huddleston, R. K. *J. Am. Chem. Soc.* **1984**, *106*, 5057. (c) Gould, I. R.; Ege, D.; Mattes, S. L.; Farid, S. *J. Am. Chem. Soc.* **1987**, *109*, 3794. (d) Ohno, T.; Yoshimura, A.; Mataga, N. *J. Phys. Chem.* **1990**, *94*, 4871.

(2) (a) Miller, J. R.; Calcaterra, L. T.; Closs, G. L. *J. Am. Chem. Soc.* **1984**, *106*, 3047. (b) Wasielewski, M. R.; Niemczyk, M. P.; Svec, W. A.; Pewitt, E. B. *J. Am. Chem. Soc.* **1985**, *107*, 1080. (c) Irvine, M. P.; Harrison, R. J.; Beddard, G. S.; Leighton, P.; Sanders, J. K. M. *Chem. Phys.* **1986**, *104*, 315. (d) McLendon, G. *Acc. Chem. Res.* **1988**, *21*, 160.

(3) (a) Marcus, R. A. *J. Chem. Phys.* **1956**, *24*, 966. (b) Marcus, R. A. *Can. J. Chem.* **1959**, *39*, 155.

(4) (a) Closs, G. L.; Calcaterra, L. T.; Green, N. J.; Penfield, K. W.; Miller, J. R. *J. Phys. Chem.* **1986**, *90*, 3673. (b) Closs, G. L.; Miller, J. R. *Science* **1988**, *240*, 440.

(5) (a) Mattes, S. L.; Farid, S. *J. Am. Chem. Soc.* **1986**, *108*, 7356. (b) Mattes, S. L.; Farid, S. In *Organic Photochemistry*; Padwa, A., Ed.; Dekker: New York, 1983; Vol. 6, p 233. (c) Fox, M. A., Channon, M. A., Eds. *Photoinduced Electron Transfer Reactions: Organic Substrates*; Elsevier: Amsterdam, 1988.

(6) Zeng, Y.; Zimmt, M. B. *J. Am. Chem. Soc.* **1991**, *113*, 5107.

(7) (a) Jortner, J. *J. Chem. Phys.* **1976**, *64*, 4860. (b) Ulstrup, J.; Jortner, J. *J. Chem. Phys.* **1975**, *63*, 4358. (c) Kestner, N. R.; Logan, J.; Jortner, J. *J. Phys. Chem.* **1974**, *78*, 2148.

(8) Zou, C.; Miers, J. B.; Ballew, R. M.; Dlott, D. D.; Schuster, G. B. *J. Am. Chem. Soc.* **1991**, *113*, 7823.

(9) (a) Miller, J. R.; Beitz, J. V. *J. Chem. Phys.* **1981**, *74*, 6746. (b) McConnel, J. *J. Chem. Phys.* **1961**, *35*, 508. (c) Larrson, S. *Discuss. Faraday Soc.* **1982**, *74*, 390.

(10) The magnitude of $|V|$ also depends on the energy gap between the initial state and the virtual superexchange states which propagate the electronic coupling.[8] Generally, this gap is different for the photoinduced charge separation and thermal charge recombination reactions.

(11) Finckh, P.; Heitele, H.; Volk, M.; Michel-Beyerle, M. E. *J. Phys. Chem.* **1988**, *92*, 6584.

(12) Liang, N.; Miller, J. R.; Closs, G. L. *J. Am. Chem. Soc.* **1989**, *111*, 8740.

(13) E_{ox}(donor) ≈ 0.87 eV; E_{red}(acceptor in 2, 3) = -1.9 eV; E_{red}(acceptor in 1) = -1.62 eV. All values referenced to Ag/AgCl.

(14) Moore, J. W.; Pearson, R. G. *Kinetics and Mechanism*; Wiley: New York, 1981; p 251.

(15) (a) Gould, I. R.; Moody, R.; Farid, S. *J. Am. Chem. Soc.* **1988**, *110*, 7242. (b) Gould, I. R.; Young, R. H.; Moody, R. E.; Farid, S. *J. Phys. Chem.* **1991**, *95*, 2068.

(16) (a) Brunschwig, B. S.; Ehrenson, S.; Sutin, N. *J. Phys. Chem.* **1986**, *90*, 3657. (b) Cannon, R. D. *Chem. Phys. Lett.* **1977**, *49*, 299. (c) Kirkwood, J. G.; Westheimer, F. H. *J. Chem. Phys.* **1938**, *6*, 506. (d) Westheimer, F. H.; Kirkwood, J. G. *J. Chem. Phys.* **1939**, *7*, 437.

(17) Marcus, R. A. *J. Phys. Chem.* **1989**, *93*, 3078.

(18) (a) Drude, P.; Nernst, W. *Z. Phys. Chem.* **1984**, *15*, 79. (b) Isaacs, N. S. *Liquid Phase High Pressure Chemistry*; Wiley-Interscience: Chichester, U.K., 1981; pp 99–101.

(19) If the true λ_s is 0.1 eV smaller than the value obtained fitting the spectrum to the single mode model, the true $\Delta G°$ will be ~ 0.1 eV more positive than the value determined from fitting.

(20) The dicyanoethylene acceptor is smaller than the dicarbomethoxyethylene acceptor. According to the Born equation,[14] the reduction potential of the smaller acceptor undergoes a larger cathodic shift in solvents less polar than ACN.

(21) Dewar, M. J. S.; Zoebisch, E. G.; Healy, E. F.; Stewart, J. P. *J. Am. Chem. Soc.* **1985,** *107,* 3902.

(22) (a) Nelsen, S. F.; Blackstock, S. C.; Kim, Y. *J. Am. Chem. Soc.* **1987,** *109,* 677. (b) Clark, T.; Nelsen, S. F. *J. Am. Chem. Soc.* **1988,** *110,* 868.

(23) Varying $\Delta G°$ by ±0.15 eV has almost no effect on the best fit value of $|V|$. However, λ_s changes in a manner that keeps the sum of $\lambda_s + \Delta G°$ constant. Only the results obtained using the value of $\Delta G°$ in Table III are reported.

(24) The optimal electron-transfer rate constant is proportional to $|V|^2$ and refers to the situation where FCWDS is 1.0.

(25) (a) Oevering, H.; Paddon-Row, M. N.; Heppener, M.; Oliver, A. M.; Cotsaris, E.; Verhoeven, J. W.; Hush, N. S. *J. Am. Chem. Soc.* **1987,** *109,* 3258. (b) Oevering, H.; Verhoeven, J. W.; Paddon-Row, M. N.; Warman, J. M. *Tetrahedron* **1989,** *45,* 4751. (c) Paddon-Row, M. N.; Oliver, A. M.; Warman, J. M.; Smit, K. J.; de Haas, M. P.; Oevering, H.; Verhoeven, J. W. *J. Phys. Chem.* **1988,** *92,* 6958. (d) Lawson, J. M.; Craig, D. C.; Paddon-Row, M. N.; Kroon, J.; Verhoeven, J. W. *Chem. Phys. Lett.* **1989,** *164,* 120. (e) Warman, J. M.; Smit, K. J.; de Haas, M. P.; Jonker, S. A.; Paddon-Row, M. N.; Oliver, A. M.; Kroon, J.; Oevering, H.; Verhoeven, J. W. *J. Phys. Chem.* **1991,** *95,* 1979. (f) Oliver, A. M.; Craig, D. C.; Paddon-Row, M. N.; Kroon, J.; Verhoeven, J. W. *Chem. Phys. Lett.* **1988,** *150,* 366.

(26) (a) Siders, P.; Cave, R. J.; Marcus, R. A. *J. Chem. Phys.* **1984,** *91,* 5613. (b) Cave, R. J.; Siders, P.; Marcus, R. A. *J. Chem. Phys.* **1986,** *90,* 1436. (c) Heiler, D.; McLendon, G.; Rogalskyj, P. *J. Am. Chem. Soc.* **1987,** *109,* 604. (d) Helms, A.; Heiler, D.; McLendon, G. *J. Am. Chem. Soc.* **1991,** *113,* 4325. (e) Sakata, Y.; Nakashima, S.; Goto, Y.; Tatemitsu, H.; Misumi, S.; Asahi, T.; Hagihara, M.; Nishikawa, S.; Okada, T.; Mataga, N. *J. Am.*

Chem. Soc. **1989,** *111,* 8979. (f) Sakata, Y.; Tsue, H.; Goto, Y.; Misumi, S.; Asahi, T.; Nishikawa, S.; Okada, T.; Mataga, N. *Chem. Lett.* **1991,** 1307.

(27) Cotton, F. A. *Chemical Applications of Group Theory,* 2nd ed.; Wiley-Interscience: New York, 1971; p 280.

(28) The importance of vibronic coupling in symmetric electron-transfer DSA molecules has been discussed by Hush. (a) Hush, N. S. In *Supramolecular Photochemistry;* Balzani, V., Reidel, D., Eds.; NATO ASI Series C; Reidel: Dordrecht, The Netherlands, 1987; pp 53–72. (b) Reimers, J. R.; Hush, N. S.; Sammeth, D. M.; Callis, P. R. *Chem. Phys. Lett.* **1990,** *169,* 622.

(29) (a) Yamagishi, A.; Iida, Y. *Bull. Chem. Soc. Jpn.* **1980,** *53,* 1340. (b) Yamagishi, A.; Watanabe, F.; Masui, T. *J. Chem. Soc., Chem. Commun.* **1977,** 274.

(30) See: refs 1b and 2d. (a) Miller, J. R.; Beitz, J. V. *J. Chem. Phys.* **1981,** *74,* 6746. (b) Beitz, J. V.; Miller, J. R. *J. Chem. Phys.* **1979,** *71,* 4579. (c) Calcaterra, L. T.; Closs, G. L.; Miller, J. R. *J. Am. Chem. Soc.* **1983,** *105,* 670. (d) Guarr, T.; McGuire, M.; Strauch, S.; McLendon, G. *J. Am. Chem. Soc.* **1983,** *105,* 616. (e) Guarr, T.; McGuire, M. E. *J. Am. Chem. Soc.* **1985,** *107,* 5104.

(31) (a) Beratan, D. N.; Onuchic, J. N. *Photosynth. Res.* **1989,** *22,* 173. (b) Onuchic, J. N.; Beratan, D. N. *J. Chem. Phys.* **1990,** *92,* 722. (c) Beratan, D. N.; Onuchic, J. N.; Betts, J. N.; Bowler, B. E.; Gray, H. B. *J. Am. Chem. Soc.* **1990,** *112,* 7915. (d) Siddarth, P.; Marcus, R. A. *J. Phys. Chem.* **1990,** *94,* 8430.

(32) Gould, I. R.; Young, R. H.; Farid, S. In *Photochemical Processes in Organized Molecular Systems;* Tazuke, S., Honda, K., Eds.; Elsevier: Amsterdam, 1990; pp 19–40.

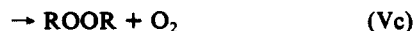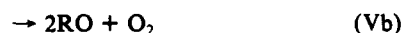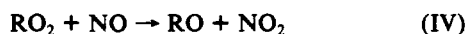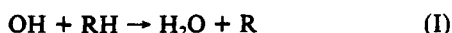# OH Radical Induced Oxidation of 2,3-Dimethylbutane in Air

Gerald Heimann and Peter Warneck*

Max-Planck-Institut für Chemie (Otto-Hahn-Institut), Mainz, Germany (Received: April 21, 1992; In Final Form: July 1, 1992)

The product distribution resulting from the OH induced oxidation of 2,3-dimethylbutane in air was measured and compared with predictions based on a general reaction mechanism. Relative rates derived for the abstraction of primary and tertiary hydrogen atoms by OH radicals from the parent compound are 17% and 83%, respectively. The branching ratio for the alcohol versus alkoxyl radical producing pathways of the self-reaction of 2-propylperoxy radicals was determined to be (0.61 ± 0.08):(0.39 ± 0.08); the corresponding ratio for the self-reaction of primary 2,3-dimethylbutylperoxy radicals is (0.56 ± 0.07):(0.44 ± 0.07). Large amounts of 2,3-dimethyl-2-hydroperoxybutane and small amounts of 2,3-dimethyl-2-butanol were found, the latter as a product of the cross combination reactions of 2,3-dimethyl-2-butylperoxy with 2-propylperoxy and 2,3-dimethyl-1-butylperoxy radicals. Rate constants of 3.5×10^{-17} and 2×10^{-16} cm^3/(molecule s), respectively, were estimated for these reactions with the help of computer simulations.

Introduction

A sound knowledge of chemical reaction mechanisms governing the low temperature oxidation of hydrocarbons in air is fundamental to any detailed considerations of the fate of a hydrocarbon in the atmosphere. Previous laboratory studies of such gas-phase oxidation processes have primarily dealt with C_1–C_4 compounds, and from this work a general reaction mechanism has been worked out that should be applicable also to higher hydrocarbons.[1-3] The oxidation of alkanes in the atmosphere is thought to start with hydrogen atom abstraction by reaction with OH radicals.[3,4] The associated rate coefficients are known in many cases. The subsequent reactions involve alkylperoxy (RO$_2$) and alkoxyl (RO) radicals as follows:

$$OH + RH \rightarrow H_2O + R \tag{I}$$

$$R + O_2 \rightarrow RO_2 \tag{II}$$

$$RO_2 + HO_2 \rightarrow ROOH \tag{III}$$

$$RO_2 + NO \rightarrow RO + NO_2 \tag{IV}$$

$$RO_2 + RO_2 \rightarrow alcohols + aldehydes/ketones + O_2 \tag{Va}$$

$$\rightarrow 2RO + O_2 \tag{Vb}$$

$$\rightarrow ROOR + O_2 \tag{Vc}$$

$$RO + O_2 \rightarrow HO_2 + aldehyde/ketone \tag{VI}$$

$$RO \rightarrow aldehyde + R' \tag{VII}$$

$$RO \rightarrow HOR'' \tag{VIII}$$

where R is the parent alkyl radical, R' is an alkyl radical of lower carbon number, and HOR'' is a hydroxyalkyl radical resulting from internal hydrogen atom abstraction by the alkoxyl group. In the polluted atmosphere, where the concentration of nitrogen oxides is fairly high, the reaction of peroxy radicals with NO (reaction IV) will dominate over all other reactions of RO$_2$ radicals. This contrasts with the background atmosphere in marine or sparsely inhabited continental regions, where the concentration of nitrogen oxides is so low that the interaction of RO$_2$ with HO$_2$ and other RO$_2$ radicals (reactions III and V) cannot be ignored.[3,5,6] For methylperoxy radicals it has been found[7,8] that the contribution of reaction Vc is small compared with reactions Va and Vb combined, and this condition is assumed to hold also in other cases. The partitioning between reactions Va and Vb as well as the degree of decomposition or rearrangement of the RO radical (reactions VII and VIII) must be determined separately for each hydrocarbon. Higher hydrocarbons allow the formation of several types of alkylperoxy radicals, which may be classified as primary,